JOURNAL OF AIRCRAFT
Vol. 37, No. 5, September–October 2000

Small Disturbance Euler Equations: Efficient and Accurate Tool for Unsteady Load Prediction

Erich Kreiselmaier* and Boris Laschka†
Technische Universität München, 85747 Garching, Germany

It is well known that the time-accurate solutions of the unsteady Euler equations are a reasonable but computationally expensive and time-consuming approach. Concerning aeroelastic applications, there is a need for efficient and accurate tools to determine the unsteady aerodynamic loads due to a variety of parameters. A numerical method based on an alternative approach, namely, on the solution of the small disturbance Euler equations (SDEu), is presented. These equations provide the following advantages: The unsteady problem is reduced to a steady-state problem for the perturbation part. The unsteady loads can be evaluated directly. Assuming harmonic behavior of unsteadiness, the use of well-proven modal methods in aeroelastic analysis is supported. By application of this method, a substantial reduction of computational time is achieved. Results are presented for several airfoils and wings in pitching motion at subsonic, transonic, and supersonic Mach numbers. It is shown that for the most critical region, namely, the transonic region, the SDEu provide an excellent and fast means for the prediction of unsteady forces. The only remarkable differences between the nonlinear Euler solution and the SDEu solution can be observed in the pressure distribution in the vicinity of a shock, which is shown to have negligible influence on the integral contribution of the shock impulse to the generalized forces.

Nomenclature

$\boldsymbol{A}$ = Jacobian matrix (ξ direction)
c = speed of sound, $\sqrt{(\gamma p/\rho)}$
$\hat{c}$ = chord length
c_L = lift coefficient
c_M = moment coefficient (about x_m)
c_p = pressure coefficient
$\hat{c}_r$ = root chord length
$\hat{c}_t$ = tip chord length
d = thickness
e = total energy per unit volume
$\boldsymbol{F}, \boldsymbol{G}, \boldsymbol{H}$ = flux vector in ξ, η, and ζ directions
Im = imaginary part, normalized with the amplitude α_1
J = Jacobian of coordinate transformation
k = nondimensional frequency
k_{red} = reduced frequency, $k/[\sqrt{(\gamma)}Ma_\infty]$
$\boldsymbol{L}$ = matrix of the left eigenvectors of the Jacobian
Ma_∞ = freestream Mach number
p = pressure
$\boldsymbol{Q}$ = conservative solution vector times J
$\boldsymbol{q}$ = conservative solution vector
$\boldsymbol{R}$ = matrix of the right eigenvectors of the Jacobian
Re = real part, normalized with the amplitude α_1
$\boldsymbol{S}$ = source term
s = half-span
U, V, W = contravariant velocities
U^*, V^*, W^* = contravariant velocities times J
u, v, w = velocity in x, y, and z directions
V = volume
x, y, z = Cartesian coordinates
x_m = axis of reference
x_p = pitching axis
α = angle of attack
γ = ratio of specific heats
δ_1 = small value
Æ = aspect ratio
Λ = diagonal matrix of the eigenvalues of the Jacobian
λ = taper ratio
ξ, η, ζ = curvilinear coordinates
ρ = density
τ = nondimensional time
τ_s = characteristic time, $\sqrt{(\gamma)}Ma_\infty \tau$
ϕ = sweep angle
Ψ = limiter function
Ψ^* = entropy correction parameter

Subscripts

k, l, m = grid index system
0 = mean value
1 = amplitude

Superscripts

$\bar{}$ = mean value
$\tilde{}$ = perturbation value
L = left value
R = right value

Introduction

THE ability to predict unsteady loads for aeroelastic calculations in an accurate and economic way is highly sought after in the aircraft industry. Modern computational fluid dynamics (CFD) codes that time accurately in advance the unsteady Euler or Navier–Stokes equations have been successfully applied in the process of aircraft development to investigate complex aerodynamics.[1,2] For aeroelastic applications, where a high number of parameters such as different natural modes, angles of attack, Mach numbers, frequencies, etc., must be investigated, such an approach is prohibitively expensive. In particular, simulations at low reduced frequencies are time consuming because, almost independent of the frequency, a periodic state can only be achieved after calculating a number of cycles.[3]

An alternative approach is the small disturbance Euler equations (SDEu). When applied to harmonic motion, they yield a set of linear variable coefficient equations for the complex amplitude of the field quantities. With this approach, first, a steady state of reference is

Presented as Paper 98-2.6.3 at the 21st Congress of the International Council of the Aeronautical Sciences, Melbourne, Victoria, Australia, 13–18 September 1998; received 14 March 1999; revision received 31 October 1999; accepted for publication 15 February 2000.

*Scientific Assistant, Lehrstuhl für Fluidmechanik.

†Full Professor, Fluid Mechanics, Lehrstuhl für Fluidmechanik. Honorary Fellow AIAA.

calculated using the nonlinear Euler equations. Second, the SDEu describing the unsteady perturbation flow are solved. In this context, they are based on an explicit harmonic perturbation, yet the examination of any other time dependency remains possible. The unsteady problem is reduced to a formal steady-state problem for the perturbation part. This leads to an efficient calculation for different frequencies and natural modes, based on one steady solution for a specific configuration. Note that the nonlinear flow physics are contained in the steady reference solution and, therefore, are also introduced into the solution for the perturbation flow. Only flows where general changes in the flow topology occur, such as occurring and vanishing shocks during one cycle, defy being correctly modeled using the SDEu.

Until the present, investigations based on the SDEu have been performed in the field of turbomachinery. Flutter and forced response in two-dimensional cascade flows were studied by Hall,[4] Hall and Crawley,[5] Hall and Clark,[6,7] and Holmes and Chuang.[8] Quasi-three-dimensional calculations have been performed by Zirkelbach[9] and Kahl and Klose,[10] as well as three-dimensional calculations by Hall and Lorence[11] and Hall et al.[12]

The methods proposed by the previous investigators mainly differ in the modeling of the shock with shock fitting or shock capturing and the formulation of the airfoil boundary condition based on a deforming or a fixed grid. For the first time, Lindquist,[13] as well as Lindquist and Giles,[14] answered the crucial question, as to what extent the SDEu equations can be applied to flows with shocks. Furthermore, their investigations of one-dimensional nozzle flows demonstrated the successful application of shock capturing. This formed the basis for the calculation of three-dimensional flows. The correct modeling of the shock impulse with respect to position and strength is necessary because its impact on unsteady loads is of the same order as the unsteady pressure distribution in the mainly linear region of the flowfield around the airfoil or wing. It was shown that by the use of shock capturing the shock impulse is smeared out and that the width and the height of the impulse depends on the amount of dissipation in the numerical scheme. Nevertheless, its contribution to the unsteady loads is not influenced by this effect.[12,13]

The formulation of the airfoil boundary condition seemed to be a crucial issue for the quality of the results. By assuming that an airfoil deforms with small amplitudes, it was reasonable to model the moving airfoil with a modified boundary condition and a fixed grid. This boundary condition requires the evaluation of the gradient of the mean flow velocity, which is difficult to compute accurately and leads to significant errors. Hence, this evaluation was neglected by some authors, though it is of great influence at the leading and trailing edges.[4,5,10,9] This deficiency has lead to the development of deforming grids and, as a consequence, to a more complicated formulation of the linearized Euler equations.

The need for an improved method for aeroelastic calculations in the transonic region suggests the use of the SDEu equations in the field of aerodynamics of aircraft. Therefore, at the Lehrstuhl für Fluidmechanik (FLM) of the Technische Universität München, the development of a CFD code based on the SDEu equations was initiated. Shock capturing is used due to its inherent simplicity for the nonlinear Euler as well as for the SDEu equations. This is accomplished with flux difference splitting according to Roe[15] and a modified MUSCL extrapolation retaining the total variation diminishing (TVD) property. The concept of deforming grids was employed to ensure an optimal evaluation of the airfoil boundary condition.

First, investigations of several airfoils (NACA 0012, NACA 64A010, and 3% parabolic) in pitching motion at subsonic, transonic, and supersonic Mach numbers are performed. Results are compared with those obtained by a nonlinear Euler method[16] and, in the subsonic case, with those of an unsteady panel method[17] as well. Second, the method is applied to three-dimensional flows, even coping with complicated shock structures. This is done for the well-known test case AGARD CT5 LANN (Lockheed-Georgia, Flight Dynamics Laboratory, NASA-Langley Research Center and National Aerospace Laboratory/NLR, see AGARD-R-702 Addendum No. 1) wing in pitching motion, which has been used for validation purposes in the framework of the European Computational Aerodynamics Research Project (ECARP).[18]

Theory

Euler Equations

In the present analysis, the unsteady compressible flow around airfoils and wings is modeled as three-dimensional, inviscid, and adiabatic. For these conditions, the governing equations are the three-dimensional Euler equations and may be expressed in strong conservation form and curvilinear coordinates for moving grids as

$$\frac{\partial \boldsymbol{Q}}{\partial \tau} + \frac{\partial \boldsymbol{F}}{\partial \xi} + \frac{\partial \boldsymbol{G}}{\partial \eta} + \frac{\partial \boldsymbol{H}}{\partial \zeta} = 0 \tag{1}$$

where $\boldsymbol{Q}$ is the vector of conservative variables times J and $\boldsymbol{F}$, $\boldsymbol{G}$, and $\boldsymbol{H}$ are the convective fluxes with respect to the ξ, η, and ζ directions:

$$\boldsymbol{Q} = J\boldsymbol{q} = J\begin{bmatrix}\rho \\ \rho u \\ \rho v \\ \rho w \\ e\end{bmatrix}, \qquad \boldsymbol{F} = J\begin{bmatrix}\rho U \\ \rho u U + \xi_x p \\ \rho v U + \xi_y p \\ \rho w U + \xi_z p \\ U(e+p) - \xi_t p\end{bmatrix}$$

$$\boldsymbol{G} = J\begin{bmatrix}\rho V \\ \rho u V + \eta_x p \\ \rho v V + \eta_y p \\ \rho w V + \eta_z p \\ V(e+p) - \eta_t p\end{bmatrix}, \qquad \boldsymbol{H} = J\begin{bmatrix}\rho W \\ \rho u W + \zeta_x p \\ \rho v W + \zeta_y p \\ \rho w W + \zeta_z p \\ W(e+p) - \zeta_t p\end{bmatrix}$$

with U, V, and W as the contravariant velocities

$$U = \xi_x u + \xi_y v + \xi_z w + \xi_t, \qquad V = \eta_x u + \eta_y v + \eta_z w + \eta_t$$
$$W = \zeta_x u + \zeta_y v + \zeta_z w + \zeta_t \tag{2}$$

If a perfect gas is assumed, the necessary closing condition is given by the equation of state,

$$p = (\gamma - 1)\left[e - \tfrac{1}{2}\rho(u^2 + v^2 + w^2)\right] \tag{3}$$

with $\gamma = c_p/c_v$.

The metric terms are defined by

$$\begin{aligned}
J\xi_x &= y_\eta z_\zeta - z_\eta y_\zeta, & J\eta_x &= z_\xi y_\zeta - y_\xi z_\zeta \\
J\xi_y &= z_\eta x_\zeta - x_\eta z_\zeta, & J\eta_y &= x_\xi z_\zeta - z_\xi x_\zeta \\
J\xi_z &= x_\eta y_\zeta - y_\eta x_\zeta, & J\eta_z &= x_\zeta y_\xi - y_\zeta x_\xi \\
J\zeta_x &= y_\xi z_\eta - z_\xi y_\eta, & \xi_t &= -x_\tau \xi_x - y_\tau \xi_y - z_\tau \xi_z \\
J\zeta_y &= x_\eta z_\xi - z_\eta x_\xi, & \eta_t &= -x_\tau \eta_x - y_\tau \eta_y - z_\tau \eta_z \\
J\zeta_z &= x_\xi y_\eta - y_\xi x_\eta, & \zeta_t &= -x_\tau \zeta_x - y_\tau \zeta_y - z_\tau \zeta_z
\end{aligned} \tag{4}$$

with

$$\begin{aligned}
J &= x_\xi J\xi_x + y_\xi J\xi_y + z_\xi J\xi_z \\
&= x_\xi(y_\eta z_\zeta - z_\eta y_\zeta) - y_\xi(x_\eta z_\zeta - z_\eta x_\zeta) + z_\xi(x_\eta y_\zeta - y_\eta x_\zeta)
\end{aligned} \tag{5}$$

On this basis, a consistent derivation of the SDEu equations that is very close to the basic formulation (1) is possible. Note that in the framework of a finite volume scheme on structured grids, J is the volume of a cell, whereas $J\xi_x$, $J\xi_y$, and $J\xi_z$ are the components of the normal cell face vector with respect to the ξ direction and $J\xi_t$ is the time rate of change of the volume due to the movement of the cell face. At the far field, characteristic boundary conditions[19] are used, which are easily adapted to the SDEu.[16]

SDEu Equations

For many aeroelastic calculations, the degree of unsteadiness of the flow is small compared to the mean flow. Therefore, the flow can be decomposed into a steady mean flow and an unsteady small perturbation flow. Furthermore, the source of unsteadiness is assumed to be harmonic, leading to the following formulation for the deforming grid:

$$
\begin{aligned}
x(\xi,\eta,\zeta,\tau) &= \bar{x}(\xi,\eta,\zeta) + \tilde{x}(\xi,\eta,\zeta)\, e^{ik\tau}\\
y(\xi,\eta,\zeta,\tau) &= \bar{y}(\xi,\eta,\zeta) + \tilde{y}(\xi,\eta,\zeta)\, e^{ik\tau}\\
z(\xi,\eta,\zeta,\tau) &= \bar{z}(\xi,\eta,\zeta) + \tilde{z}(\xi,\eta,\zeta)\, e^{ik\tau}
\end{aligned}
\tag{6}
$$

where $\tilde{x}$, $\tilde{y}$, and $\tilde{z}$ are the amplitude of grid motion about the steady reference positions $\bar{x}$, $\bar{y}$, and $\bar{z}$ and k is the nondimensional frequency parameter with respect to the nondimensional time τ. With these assumptions, the metrics of steady state and the metrics of the perturbation, undergoing harmonic variations as well, can be derived. For the sake of brevity, this is shown only for the metrics in ξ direction:

$$
\begin{aligned}
&J\xi_x = \overline{J\xi_x} + \widetilde{J\xi_x}\, e^{ik\tau}, \qquad J\xi_y = \overline{J\xi_y} + \widetilde{J\xi_y}\, e^{ik\tau}\\
&J\xi_z = \overline{J\xi_z} + \widetilde{J\xi_z}\, e^{ik\tau}, \qquad J\xi_t = \overline{J\xi_t} + \widetilde{J\xi_t}\, e^{ik\tau}, \qquad J = \bar{J} + \tilde{J}\, e^{ik\tau}
\end{aligned}
\tag{7}
$$

with

$$
\widetilde{J\xi_x} = \bar{y}_\eta\tilde{z}_\zeta - \bar{z}_\eta\tilde{y}_\zeta + \tilde{y}_\eta\bar{z}_\zeta - \tilde{z}_\eta\bar{y}_\zeta
$$

$$
\widetilde{J\xi_y} = \bar{z}_\eta\tilde{x}_\zeta - \bar{x}_\eta\tilde{z}_\zeta + \tilde{z}_\eta\bar{x}_\zeta - \tilde{x}_\eta\bar{z}_\zeta
$$

$$
\widetilde{J\xi_z} = \bar{x}_\eta\tilde{y}_\zeta - \bar{y}_\eta\tilde{x}_\zeta + \tilde{x}_\eta\bar{y}_\zeta - \tilde{y}_\eta\bar{x}_\zeta
$$

$$
\widetilde{J\xi_t} = -ik\tilde{x}\overline{J\xi_x} - ik\tilde{y}\overline{J\xi_y} - ik\tilde{z}\overline{J\xi_z}
$$

$$
\tilde{J} = \bar{x}_\xi\widetilde{J\xi_x} + \bar{y}_\xi\widetilde{J\xi_y} + \bar{z}_\xi\widetilde{J\xi_z} + \tilde{x}_\xi\overline{J\xi_x} + \tilde{y}_\xi\overline{J\xi_y} + \tilde{z}_\xi\overline{J\xi_z} \tag{8}
$$

In a similar way, the unsteady field quantities are defined by the superposition of a steady and a perturbation state:

$$
\boldsymbol{q}(\xi,\eta,\zeta) = \bar{\boldsymbol{q}}(\xi,\eta,\zeta) + \tilde{\boldsymbol{q}}(\xi,\eta,\zeta)\, e^{ik\tau} \tag{9}
$$

Now the perturbation expressions of the grid, the metrics, and the field quantities are substituted into the Euler equations in strong conservation form and curvilinear coordinates (1). Collecting the terms of zero order leads to the nonlinear steady-state Euler equations, equivalent to the steady version of Eq. (1) and all quantities marked with an overbar. After some manipulation, collecting the terms of first order results in the SDEu equations

$$
\frac{\partial\tilde{\boldsymbol{Q}}^{(1)}}{\partial\tau} + \frac{\partial\tilde{\boldsymbol{F}}^{(1)}}{\partial\xi} + \frac{\partial\tilde{\boldsymbol{G}}^{(1)}}{\partial\eta} + \frac{\partial\tilde{\boldsymbol{H}}^{(1)}}{\partial\zeta} = -\left(\tilde{\boldsymbol{Q}}^{(1)}ik + \tilde{\boldsymbol{Q}}^{(2)}ik + \frac{\partial\tilde{\boldsymbol{F}}^{(2)}}{\partial\xi} + \frac{\partial\tilde{\boldsymbol{G}}^{(2)}}{\partial\eta} + \frac{\partial\tilde{\boldsymbol{H}}^{(2)}}{\partial\zeta}\right) \tag{10}
$$

$$
\tilde{\boldsymbol{Q}}^{(1)} = \bar{J}\tilde{\boldsymbol{q}} = \begin{bmatrix} \bar{J}\tilde{\rho}\\ \bar{J}\widetilde{\rho u}\\ \bar{J}\widetilde{\rho v}\\ \bar{J}\widetilde{\rho w}\\ \bar{J}\tilde{e} \end{bmatrix}, \qquad \tilde{\boldsymbol{F}}^{(1)} = \left.\frac{\partial\boldsymbol{F}}{\partial\boldsymbol{q}}\right|_{\bar{q}}\tilde{\boldsymbol{q}} = \bar{\boldsymbol{A}}\tilde{\boldsymbol{q}}
$$

$$
\tilde{\boldsymbol{Q}}^{(2)} = \begin{bmatrix} \tilde{J}\bar{\rho}\\ \tilde{J}\overline{\rho u}\\ \tilde{J}\overline{\rho v}\\ \tilde{J}\overline{\rho w}\\ \tilde{J}\bar{e} \end{bmatrix}, \qquad \tilde{\boldsymbol{F}}^{(2)} = \begin{bmatrix} \bar{\rho}\tilde{U}^*\\ \overline{\rho u}\tilde{U}^* + \widetilde{J\xi_x}\bar{p}\\ \overline{\rho v}\tilde{U}^* + \widetilde{J\xi_y}\bar{p}\\ \overline{\rho w}\tilde{U}^* + \widetilde{J\xi_z}\bar{p}\\ \tilde{U}^*(\bar{e}+\bar{p}) - \widetilde{J\xi_t}\bar{p} \end{bmatrix}
$$

with

$$
\tilde{U}^* = \widetilde{J\xi_x}\bar{u} + \widetilde{J\xi_y}\bar{v} + \widetilde{J\xi_z}\bar{w} + \widetilde{J\xi_t}
$$

$$
\bar{\boldsymbol{A}} = \begin{bmatrix}
0 & \overline{J\xi_x} & \overline{J\xi_y} & \overline{J\xi_z} & 0\\
\overline{J\xi_x}\bar{\phi} - \bar{u}\bar{U}^* & \bar{U}^* + (2-\gamma)\overline{J\xi_x}\bar{u} & \overline{J\xi_y}\bar{u} - (\gamma-1)\overline{J\xi_x}\bar{v} & \overline{J\xi_z}\bar{u} - (\gamma-1)\overline{J\xi_x}\bar{w} & (\gamma-1)\overline{J\xi_x}\\
\overline{J\xi_y}\bar{\phi} - \bar{v}\bar{U}^* & \overline{J\xi_x}\bar{v} - (\gamma-1)\overline{J\xi_y}\bar{u} & \bar{U}^* + (2-\gamma)\overline{J\xi_y}\bar{v} & \overline{J\xi_z}\bar{v} - (\gamma-1)\overline{J\xi_y}\bar{w} & (\gamma-1)\overline{J\xi_y}\\
\overline{J\xi_z}\bar{\phi} - \bar{w}\bar{U}^* & \overline{J\xi_x}\bar{w} - (\gamma-1)\overline{J\xi_z}\bar{u} & \overline{J\xi_y}\bar{w} - (\gamma-1)\overline{J\xi_z}\bar{v} & \bar{U}^* + (2-\gamma)\overline{J\xi_z}\bar{w} & (\gamma-1)\overline{J\xi_z}\\
(2\bar{\phi} - \gamma\bar{e}/\bar{\rho})\bar{U}^* & (\gamma\bar{e}/\bar{\rho} - \bar{\phi})\overline{J\xi_x} - (\gamma-1)\bar{U}^*\bar{u} & (\gamma\bar{e}/\bar{\rho} - \bar{\phi})\overline{J\xi_y} - (\gamma-1)\bar{U}^*\bar{v} & (\gamma\bar{e}/\bar{\rho} - \bar{\phi})\overline{J\xi_z} - (\gamma-1)\bar{U}^*\bar{w} & \gamma\bar{U}^*
\end{bmatrix}
$$

$$
\bar{U}^* = \overline{J\xi_x}\bar{u} + \overline{J\xi_y}\bar{v} + \overline{J\xi_z}\bar{w}, \qquad \bar{\phi} = [(\gamma-1)/2](\bar{u}^2 + \bar{v}^2 + \bar{w}^2)
$$

The first term of Eq. (10) is due to the perturbation amplitude $\tilde{\boldsymbol{q}}$ being assumed to be formally time dependent. Hence, one obtains a time-dependent numerical scheme that is characterized by pseudotime marching. Homogeneous terms in $\tilde{\boldsymbol{q}}$ are marked with superscript (1) and inhomogeneous terms with (2). It becomes evident from the preceding equations that an unsteady solution evolves solely from the unsteady metrics in the inhomogeneous terms by causing an interaction of the real and imaginary parts of the SDEu. This interaction is removed in the quasi-steady case, that is, $k = 0$. Finally, the linearized form of the equation of state is given by

$$
\tilde{p} = (\gamma-1)\left[\tilde{e} - \tfrac{1}{2}\left(2\bar{u}\widetilde{\rho u} - \bar{u}^2\tilde{\rho} + 2\bar{v}\widetilde{\rho u} - \bar{v}^2\tilde{\rho} + 2\bar{w}\widetilde{\rho u} - \bar{w}^2\tilde{\rho}\right)\right] \tag{11}
$$

Numerical Procedure

First, a grid for the mean flow, as well as a grid that represents the perturbation due to a given deformation of the surface, is obtained by employing an elliptic grid generator. Second, the mean flow is computed using a finite volume approach relying on Roe's flux difference splitting.[15] Second-order accuracy is achieved by MUSCL extrapolation of the conservative variables, also ensuring the TVD property. Time integration can be performed in an explicit or implicit manner. For three-dimensional calculations, the lower–upper symmetric-successive-overrelaxation (LU-SSOR) scheme, first introduced by Jameson and Turkel,[20] is used.

With the exception of a source term, the SDEu (10) are formally equivalent to the original Euler equations (1), resulting in a similar derivation of the discretized equations. Therefore, the SDEu are replaced by the following semidiscretized equation with the right-hand side:

$$\frac{\partial \tilde{\boldsymbol{Q}}^{(1)}_{k,l,m}}{\partial \tau} = -\boldsymbol{RHS}_{k,l,m}$$

$$\boldsymbol{RHS}_{k,l,m} = \tilde{\boldsymbol{F}}^{(1)}_{k+\frac{1}{2},l,m} - \tilde{\boldsymbol{F}}^{(1)}_{k-\frac{1}{2},l,m} + \tilde{\boldsymbol{G}}^{(1)}_{k,l+\frac{1}{2},m} - \tilde{\boldsymbol{G}}^{(1)}_{k,l-\frac{1}{2},m} + \tilde{\boldsymbol{H}}^{(1)}_{k,l,m+\frac{1}{2}} - \tilde{\boldsymbol{H}}^{(1)}_{k,l,m-\frac{1}{2}} - \tilde{\boldsymbol{S}}^{(1)}_{k,l,m} - \tilde{\boldsymbol{S}}^{(2)}_{k,l,m}$$

$$\tilde{\boldsymbol{Q}}^{(1)}_{k,l,m} = \bar{V}_{k,l,m}\tilde{\boldsymbol{q}}_{k,l,m} \tag{12}$$

where $\tilde{\boldsymbol{S}}^{(1)}_{k,l,m}$ is the homogeneous part and $\tilde{\boldsymbol{S}}^{(2)}_{k,l,m}$ the inhomogeneous part of the source term,

$$\tilde{\boldsymbol{S}}^{(1)}_{k,l,m} = -\tilde{\boldsymbol{Q}}^{(1)}_{k,l,m} ik$$

$$\tilde{\boldsymbol{S}}^{(2)}_{k,l,m} = -\Big(\tilde{\boldsymbol{Q}}^{(2)}_{k,l,m} ik + \tilde{\boldsymbol{F}}^{(2)}_{k+\frac{1}{2},l,m} - \tilde{\boldsymbol{F}}^{(2)}_{k-\frac{1}{2},l,m} + \tilde{\boldsymbol{G}}^{(2)}_{k,l+\frac{1}{2},m} - \tilde{\boldsymbol{G}}^{(2)}_{k,l-\frac{1}{2},m} + \tilde{\boldsymbol{H}}^{(2)}_{k,l,m+\frac{1}{2}} - \tilde{\boldsymbol{H}}^{(2)}_{k,l,m-\frac{1}{2}}\Big) \tag{13}$$

The main focus is on the consistent deduction of a linearized Roe flux difference splitting. The numerical flux $\tilde{\boldsymbol{F}}^{(1)}_{k+1/2}$ (for the sake of clarity triple indexing is omitted) is given by

$$\tilde{\boldsymbol{F}}^{(1)}_{k+\frac{1}{2}} = \tfrac{1}{2}\Big[\Big(\boldsymbol{A}^{(1)L}_{k+\frac{1}{2}} + \boldsymbol{R}^{(1)}_{k+\frac{1}{2}}\Big|\bar{\Lambda}_{k+\frac{1}{2}}\Big|\boldsymbol{L}^{(1)}_{k+\frac{1}{2}}\Big)\tilde{\boldsymbol{q}}^{L}_{k+\frac{1}{2}} + \Big(\boldsymbol{A}^{(1)R}_{k+\frac{1}{2}} - \boldsymbol{R}^{(1)}_{k+\frac{1}{2}}\Big|\bar{\Lambda}_{k+\frac{1}{2}}\Big|\boldsymbol{L}^{(1)}_{k+\frac{1}{2}}\Big)\tilde{\boldsymbol{q}}^{R}_{k+\frac{1}{2}}\Big] \tag{14}$$

where $\boldsymbol{A}^{(1)L/R}_{k+1/2}$ are the Jacobian matrices evaluated with the steady-state field quantities of the left/right side of the cell interface. However, the matrices of the left and right eigenvectors $\boldsymbol{L}^{(1)}_{k+1/2}$ and $\boldsymbol{R}^{(1)}_{k+1/2}$, as well as the diagonal matrix $\bar{\Lambda}_{k+1/2}$, that contain the eigenvalues of the Jacobian matrix $\bar{\boldsymbol{A}}$ are evaluated with the Roe averages. To maintain consistency to the basic nonlinear Euler solver, the eigenvalues are corrected corresponding to Harten[21] and Yee[22] with a continously differentiable approximation of the absolute value function

$$\Psi^*(z) = \begin{cases} |z| & |z| \geq \delta \\ (z^2+\delta^2)/2\delta & |z| < \delta \end{cases} \tag{15}$$

where δ is a parameter that is obtained by scaling the largest eigenvalue

$$\delta = \delta_1 \cdot (|U| + c|\nabla\xi|) \tag{16}$$

Furthermore MUSCL extrapolation is used to calculate the left and right steady-state conservative field quantities $\bar{q}$

$$\bar{q}^L_{k+\frac{1}{2}} = \bar{q}_k + \tfrac{1}{2}\bar{\Psi}^L_{k+\frac{1}{2}}(\bar{q}_k - \bar{q}_{k-1})$$

$$\bar{q}^R_{k+\frac{1}{2}} = \bar{q}_{k+1} + \tfrac{1}{2}\bar{\Psi}^R_{k+\frac{1}{2}}(\bar{q}_{k+2} - \bar{q}_{k+1}) \tag{17}$$

$$\bar{\Psi}^L_{k+\frac{1}{2}} = \Psi\Big(\bar{r}^L_{k+\frac{1}{2}}\Big) \qquad \bar{r}^L_{k+\frac{1}{2}} = \frac{\bar{q}_{k+1}-\bar{q}_k}{\bar{q}_k - \bar{q}_{k-1}}$$

$$\bar{\Psi}^R_{k+\frac{1}{2}} = \Psi\Big(\bar{r}^R_{k+\frac{1}{2}}\Big) \qquad \bar{r}^R_{k+\frac{1}{2}} = \frac{\bar{q}_{k+1}-\bar{q}_k}{\bar{q}_{k+2} - \bar{q}_{k+1}} \tag{18}$$

For all calculations, the Van Albada limiter

$$\Psi = (r^2 + r)/(r^2+1) \tag{19}$$

is implemented. Linearizing the MUSCL extrapolation up to first order leads to

$$\tilde{q}^L_{k+\frac{1}{2}} = \tilde{q}_k + \tfrac{1}{2}\bar{\Psi}^L_{k+\frac{1}{2}}(\tilde{q}_k - \tilde{q}_{k-1}) + \tfrac{1}{2}\tilde{\Psi}^L_{k+\frac{1}{2}}(\bar{q}_k - \bar{q}_{k-1})$$

$$\tilde{q}^R_{k+\frac{1}{2}} = \tilde{q}_{k+1} + \tfrac{1}{2}\bar{\Psi}^R_{k+\frac{1}{2}}(\tilde{q}_{k+2} - \tilde{q}_{k+1}) + \tfrac{1}{2}\tilde{\Psi}^R_{k+\frac{1}{2}}(\bar{q}_{k+2} - \bar{q}_{k+1}) \tag{20}$$

including a perturbation of the limiter. To maintain simplicity and to allow the application of not continously differentiable limiters, the perturbation of the limiter $\tilde{\Psi}^{L/R}$ is omitted. Nevertheless, a drawback in accuracy supposedly appears only in regions of strong nonlinearity.

The source term $\tilde{\boldsymbol{S}}^{(2)}_{k,l,m}$ is computed once at the beginning of the SDEu calculation from the known steady-state solution and the perturbation metrics of the prescribed grid motion. The numerical flux $\tilde{\boldsymbol{F}}^{(2)}_{k+1/2}$ is

$$\tilde{\boldsymbol{F}}^{(2)}_{k+\frac{1}{2}} = \tfrac{1}{2}\Big[\tilde{\boldsymbol{F}}^{(2)}\Big(\bar{\boldsymbol{q}}^L_{k+\frac{1}{2}}\Big) + \tilde{\boldsymbol{F}}^{(2)}\Big(\bar{\boldsymbol{q}}^R_{k+\frac{1}{2}}\Big) - \boldsymbol{R}^{(2)}_{k+\frac{1}{2}}\Big|\tilde{\Lambda}_{k+\frac{1}{2}}\Big|\boldsymbol{L}^{(2)}_{k+\frac{1}{2}}\Big(\bar{\boldsymbol{q}}^R_{k+\frac{1}{2}} - \bar{\boldsymbol{q}}^L_{k+\frac{1}{2}}\Big)\Big] \tag{21}$$

It is important to emphasize that the entropy correction has to be linearized to apply it to the linearized eigenvalues in the diagonal matrix $|\tilde{\Lambda}_{k+1/2}|$

$$\tilde{\Psi}^*(\bar{z},\tilde{z}) = \begin{cases} (\bar{z}/|\bar{z}|)\tilde{z} & |\bar{z}| \geq \delta \\ (\bar{z}/\delta)\tilde{z} & |\bar{z}| < \delta \end{cases} \tag{22}$$

Disregarding this linearization has a strong impact on the quality of the results.

Results and Discussion

Results for two- and three-dimensional cases are presented. For two-dimensional flow, a NACA 0012 airfoil is investigated in the subsonic region, a NACA 64A010 airfoil in the transonic region, and a 3% parabolic airfoil in the supersonic region, in each case performing a pitching oscillation. In the three-dimensional case, the pitching oscillation of the LANN wing is investigated for a transonic Mach number. The results of SDEu are compared with the corresponding nonlinear Euler method and, in the subsonic two-dimensional case, with an unsteady panel method.[17] In all figures, the different methods are denoted as follows: FLM-SDEu corresponds to the SDEu method, FLM-Eu to the nonlinear Euler method, and Potential to the described panel method.

Pitching NACA 0012 Airfoil in the Subsonic Region

For the NACA 0012 airfoil (Fig. 1), first, the SDEu are applied to a flow that is governed by linear flow physics. The motion of the airfoil is given by

$$\alpha(\tau_s) = \alpha_0 + \alpha_1 \sin(k_{\text{red}} \cdot \tau_s) \tag{23}$$

and the simulation parameters are $Ma_\infty = 0.5$, $k_{\text{red}} = 0.0 - 4.0$, $x_p/\hat{c} = 0.5$, $x_m/\hat{c} = 0.5$, $\alpha_0 = 0.0$ deg, and $\alpha_1 = 1.0$ deg (Figs. 2

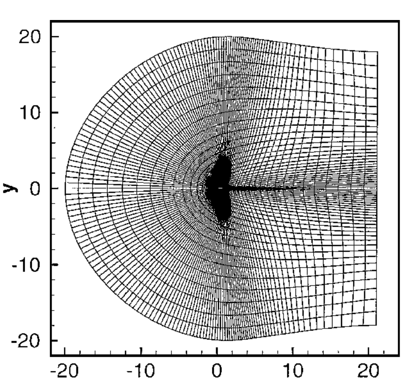

Fig. 1 C grid for the NACA 0012 airfoil.

and 3). The Euler calculations were carried out on a fairly coarse C-type grid with 180 cells in the wraparound, 30 cells in the normal direction, and a far-field distance of 20 chord lengths (Fig. 1). Figure 2 shows the first harmonic of the unsteady lift and moment coefficient and Fig. 3 the corresponding first harmonic of the unsteady pressure distribution at the reduced frequency $k_{\text{red}} = 2.5$. The conformity between the SDEu and the nonlinear Euler method is excellent for the frequency range considered. With increased frequency, a significant difference between the Euler methods and the potential method can be observed, caused by the dissimilar numerical approaches, as becomes evident in the solution at the trailing edge. Euler methods exhibit a certain amount of numerical viscosity leading to an inherent formulation of the Kutta condition and a smooth pressure distribution. In a potential method this has to be done explicitly, leading to a strong recovery of pressure at the trailing edge. Therefore, unsteady changes have a strong impact on the whole pressure distribution.

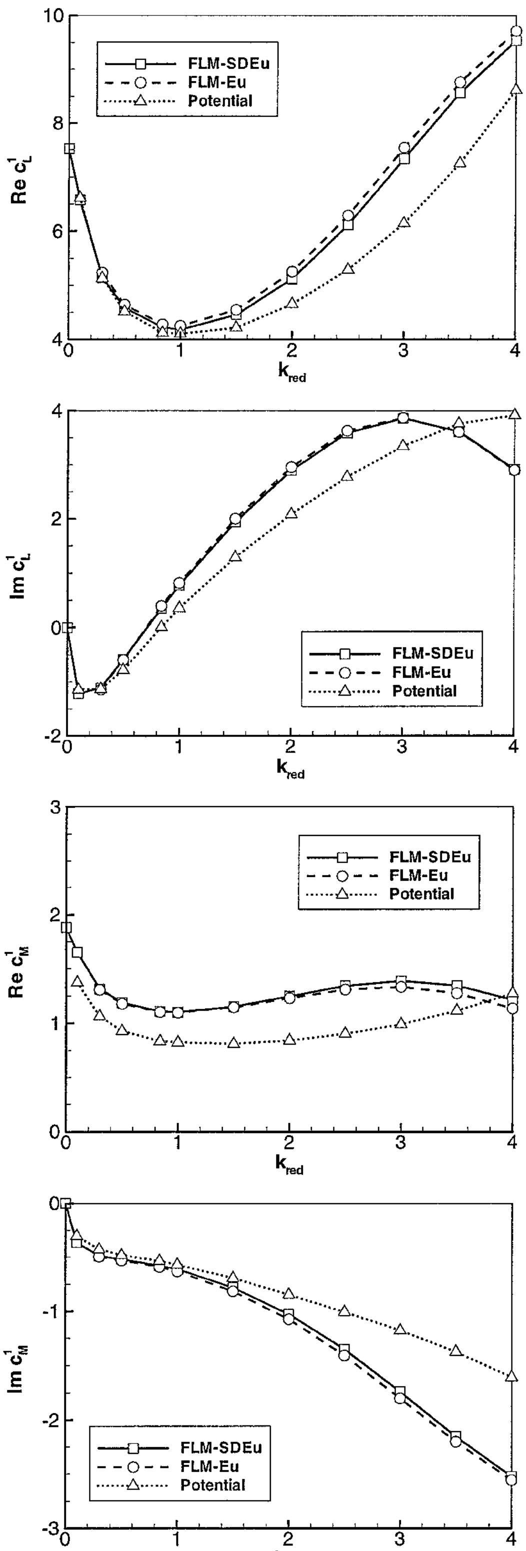

Fig. 2 NACA 0012: pitching oscillation, real and imaginary part of the first harmonic of c_L and c_M, symbols indicate the calculated frequencies.

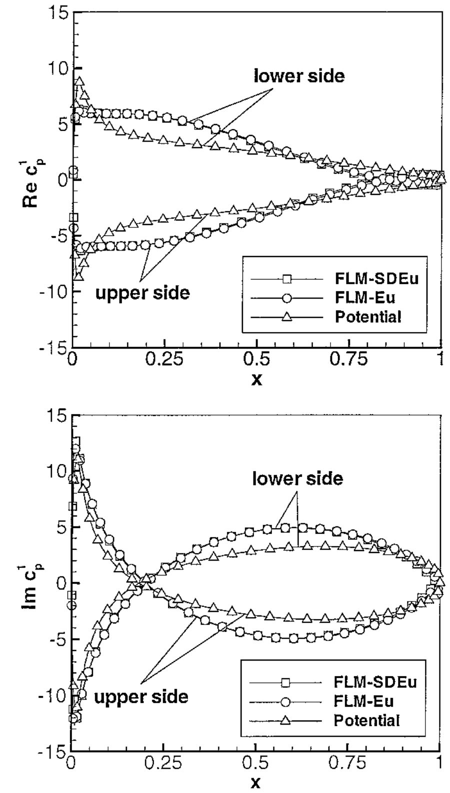

Fig. 3 NACA 0012: pitching oscillation, real and imaginary part of the first harmonic of c_p, symbols indicate each second discretized point.

Pitching NACA 64A010 Airfoil in the Transonic Region

To display the capabilities of the presented method in the critical transonic region, the well-known transonic test case NACA 64A010 airfoil in pitching motion[23] with $Ma_\infty = 0.796$, $k_{\text{red}} = 0.05$–0.606, $x_p/\hat{c} = 0.25$, $x_m/\hat{c} = 0.25$, $\alpha_0 = 0.0$ deg, and $\alpha_1 = 1.0$ deg is presented (Figs. 4 and 5). Again a C-type grid with the same parameters as for the NACA 0012 airfoil is used. To adapt the grid to the expected flow, it is refined in the region of the shock motion. Figure 4 shows the zero and first harmonic of the pressure distribution for $k_{\text{red}} = 0.404$. Note that c_p^0 of the SDEu and the experiment are steady-state values. Up to the shock region, the conditions for linearization are excellent. The agreement of the numerical results for c_p^0 with the experimental results is extremely good in the shock region and downstream. Differences for c_p^0 are observed upstream of the shock due to wind-tunnel wall effects.[24]

The first harmonic of the pressure distribution conforms very well up to the shock region, where deviations between SDEu and the nonlinear Euler code can be detected. In spite of differences in the shape of the shock impulse to be found in the local pressure distributions, the load contribution of the shock impulses can be considered equal.

The first harmonic of the lift coefficient in Fig. 5, as evaluated by SDEu, conforms very well with the equivalent result of the nonlinear code. This is remarkable, because shock movement covers a region of about 20% of the chord length depending on the frequency. This verifies the equivalent impact of shock impulses, originally introduced by Lindquist and Giles.[14] Therefore, shock capturing is

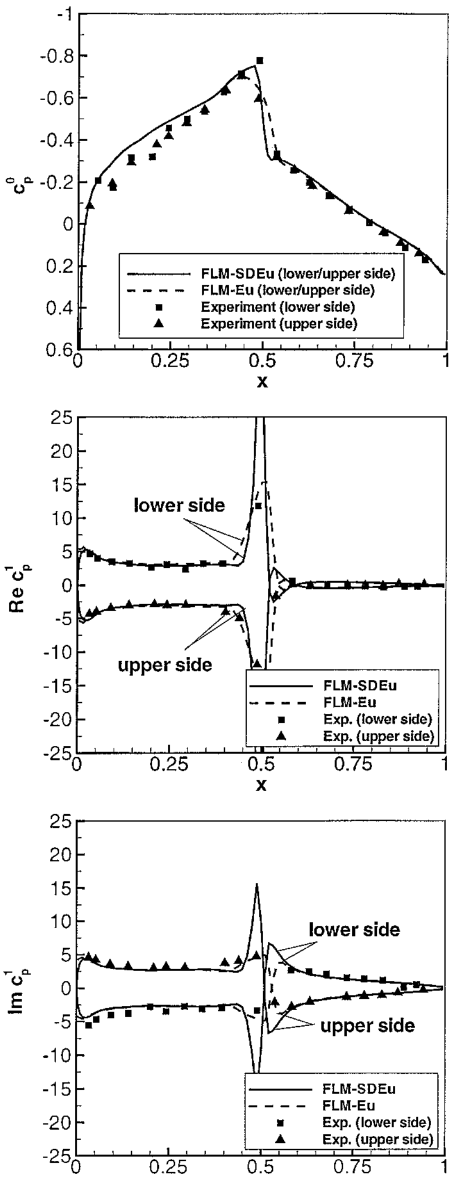

Fig. 4 NACA 64A010: pitching oscillation, zero harmonic and real and imaginary part of the first harmonic of c_p.

an appropriate approach even for the SDEu equations making transonic, three-dimensional applications possible where shock fitting would be unfeasible.

Pitching 3% Parabolic Airfoil in the Supersonic Region

For the supersonic case, the SDEu equations are employed to a 3% parabolic airfoil. The existence of a sharp leading edge and trailing edge implies the use of an H-type grid. It is composed of two blocks with 120×30 cells each and with 60 cells on every side of the airfoil. The simulation parameters are given by $Ma_\infty = 1.4$, $k_{\text{red}} = 0.0\text{–}2.0$, $x_p/\hat{c} = 0.5$, $x_m/\hat{c} = 0.5$, $\alpha_0 = 0.0$ deg, and $\alpha_1 = 1.0$ deg (Fig. 6). In this case, the shocks are fixed to the leading and trailing edge, resulting in excellent conformity not only for the coefficients (Fig. 6), but also for the unsteady pressure distribution, shown in Fig. 7 for $k_{\text{red}} = 1.0$.

Pitching LANN Wing in the Transonic Region

As an example for three-dimensional calculations the LANN wing in transonic flow is selected. Within the ECARP,[18] the AGARD CT5 test case is subject to extensive investigations with different CFD codes. Geometric parameters of the wing are given in Table 1. The simulation parameters are $Ma_\infty = 0.82$,

Table 1 Geometric parameters of the LANN wing

Parameter	Value	Parameter	Value
$\hat{c}_r$	1.0	$Æ$	7.92
s	2.77	$\lambda = \hat{c}_t/\hat{c}_r$	0.4
$d/\hat{c}$	12%	$\phi_{0.25}$	25 deg

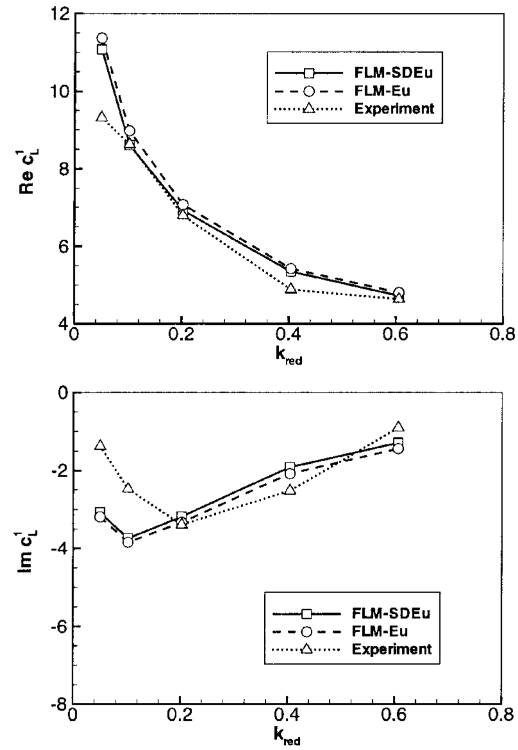

Fig. 5 NACA 64A010: pitching oscillation, real and imaginary part of the first harmonic of c_L, symbols indicate the calculated frequencies.

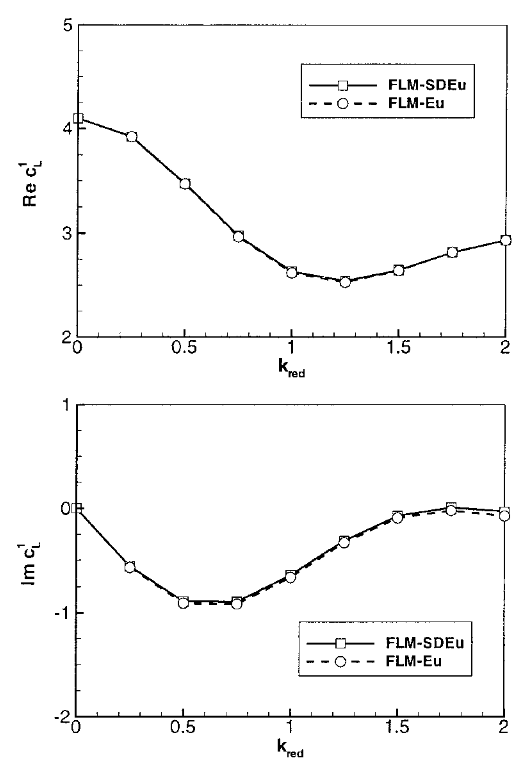

Fig. 6 Airfoil 3% parabolic: pitching oscillation, real and imaginary part of the first harmonic of c_L, symbols indicate the calculated frequencies.

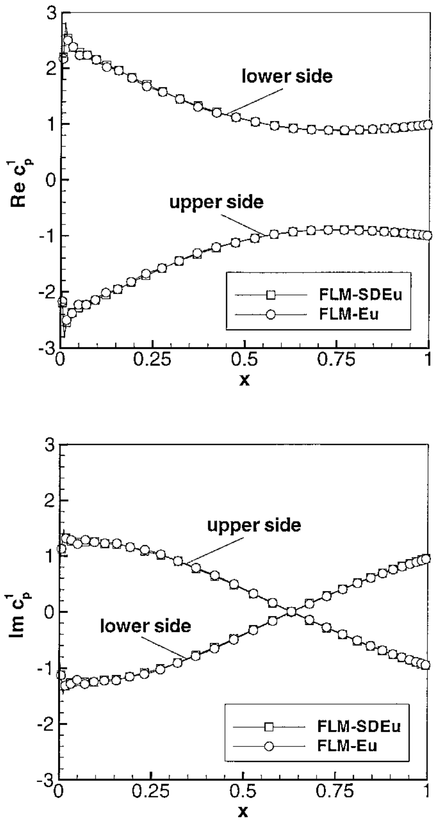

Fig. 7 Airfoil 3% parabolic: pitching oscillation, real and imaginary part of the first harmonic of c_p, symbols indicate each second discretized point.

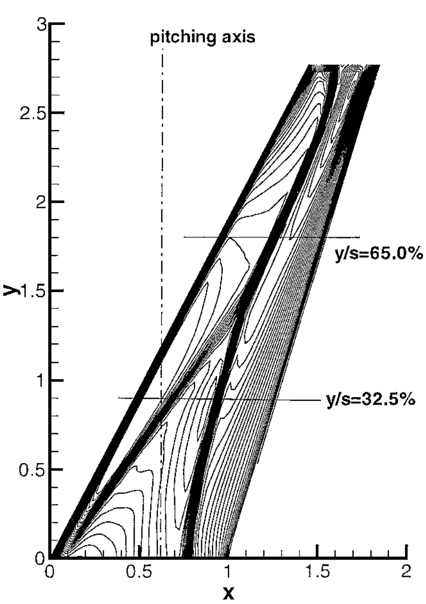

Fig. 8 LANN wing: steady flow contour lines of the steady c_p distribution (Δc_p = 0.025) on the upper surface of the wing.

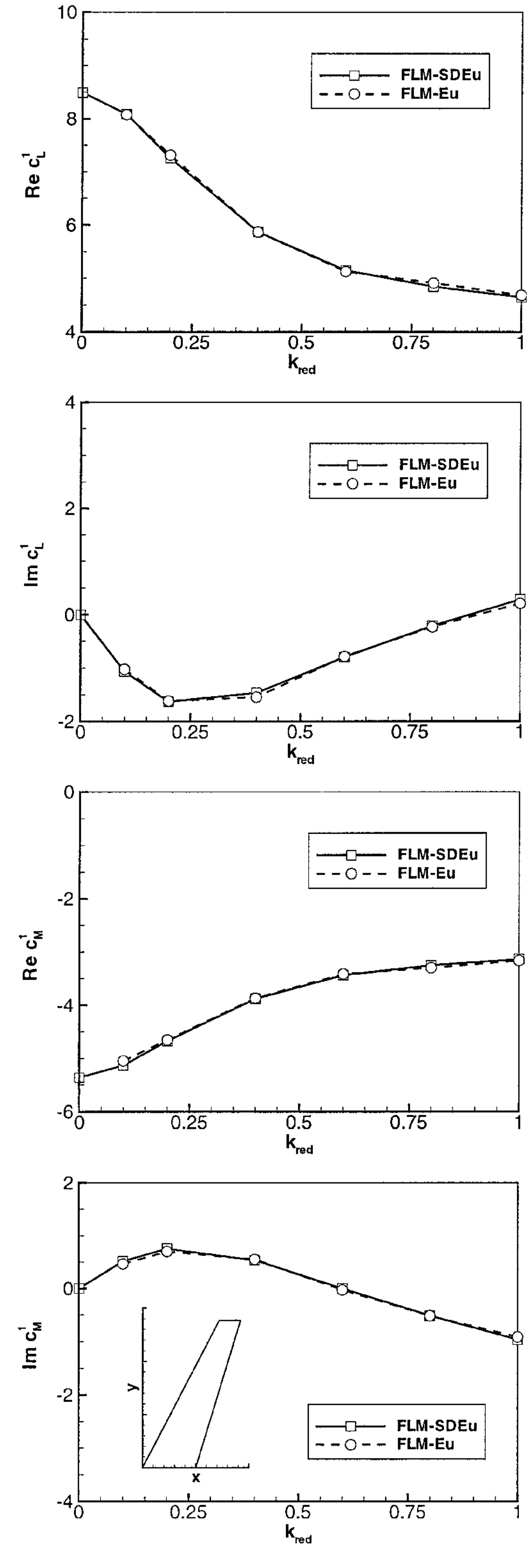

Fig. 9 LANN wing: pitching oscillation, real and imaginary part of the first harmonic of c_L and c_M, symbols indicate the calculated frequencies.

$k_{\text{red}} = 0.0$–1.0, $x_p/\hat{c}_r = 0.621$, $x_m/\hat{c} = 0.25$, $\alpha_0 = 0.6$ deg, and $\alpha_1 = 0.25$ deg (Figs. 8 and 9).

The simulation is done on a CH-type grid with $160 \times 32 \times 40$ cells, as suggested by ECARP. Lower and upper surfaces are discretized with 60×28 cells. The upper side of the wing shows a λ-shock system (Fig. 8). Figure 9 shows the unsteady lift and moment coefficients, obtained with the SDEu and the nonlinear Euler method, for the considered range of frequency. The agreement is excellent even for a complicated shock structure. This is confirmed by a more detailed analysis of the zero and first harmonic of the pressure distributions for $k_{\text{red}} = 0.204$ at two different spanwise sections $y/s = 32.5$ and 65%, shown in Figs. 10 and 11. The SDEu and the nonlinear FLM-Eu code are compared with the codes of two ECARP partners, namely, the DLR Institute of Aeroelasticity (DLR AE) and the DLR Institute of Design Aerodynamics (DLR EA). The zero harmonic of the pressure coefficient (Fig. 10)

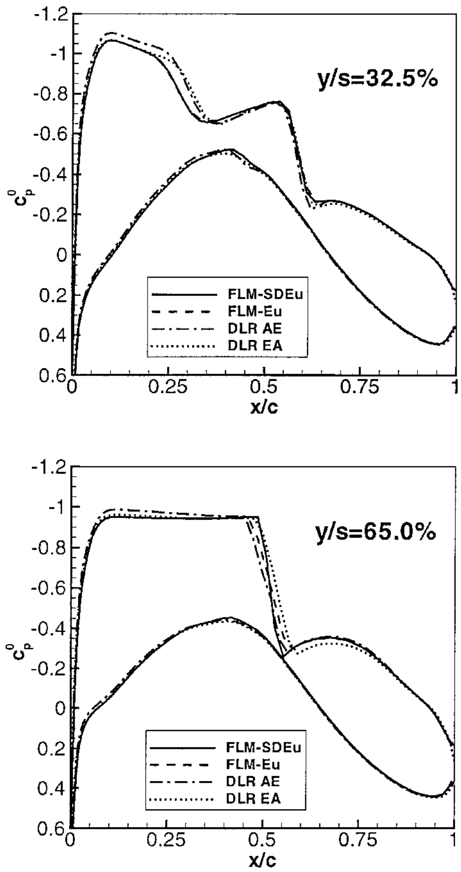

Fig. 10 LANN wing: pitching oscillation (Ma_∞ = 0.82, k_{red} = 0.204, α_0 = 0.6 deg, α_1 = 0.25 deg), zero harmonic of c_p.

exhibits excellent agreement between FLM-SDEu and FLM-Eu at the section y/s = 32.5% even in the shock region. This can be attributed to the recompression occurring over the two shocks, their individual strength being weaker than the single shock at section y/s = 65.0%. At this section, a significant difference occurs only at the shock. This shows that with the exception of the shock region the flow physics are linear. Because of different amounts of numerical viscosity, a shock displacement of about 2% between the various nonlinear Euler codes is observed at the first shock of the inner section. Nevertheless, the overall agreement of the authors' results with these results is very good. The first harmonics of the pressure distribution of SDEu and nonlinear Euler (Fig. 11) conform very well. As already explained, in the two-dimensional case the shock impulse exhibits some variation, but the contribution to the unsteady load is equal. With respect to the results of DLR EA and DLR AE, deviations occur other than just at the shocks. The displacement of the shock impulse belonging to the shock at section y/s = 32.5% corresponds to the differences in the shock position, as seen in Fig. 10. Figure 11 clearly shows that the variations in the computational results due to numerical modeling are more significant than the differences obtained with the SDEu or the nonlinear Euler method. That means that the SDEu code provides high-quality results and is suitable for the description of unsteady flows, due to the direct determination of the unsteady flow part.

Note that the SDEu only needed $\frac{1}{10}$th of the time required by the corresponding nonlinear Euler code to achieve the solution. For the unsteady simulation with the nonlinear Euler code dual time stepping was applied. Each cycle was subdivided into 160 physical time steps; for three oscillation cycles about 42,000 iterations were necessary. For the SDEu, code convergence is achieved after 8300 iterations. On a VPP 700, the steady solution for the LANN wing was obtained within 90 CPU min. The unsteady solution requires 1300 CPU min using the nonlinear Euler code and 150 CPU min using the SDEu code.

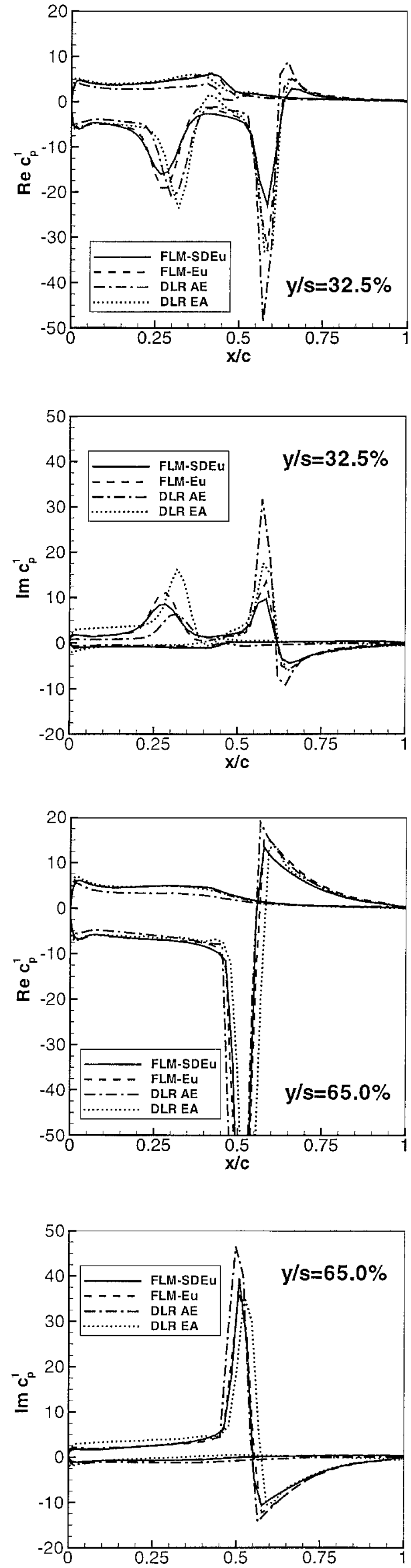

Fig. 11 LANN wing: pitching oscillation (Ma_∞ = 0.82, k_{red} = 0.204, α_0 = 0.6 deg, α_1 = 0.25 deg), real and imaginary part of the first harmonic of c_p.

Conclusions

A new consistent linearization of the unsteady three-dimensional nonlinear Euler equations is presented, leading to a set of linear variable coefficient equations, SDEu. The benefits of the SDEu are as follows.

1) The harmonic behavior reduces the solution to a steady-state problem for the amplitudes of the unsteady air forces.

2) The separation of steady and unsteady terms in the Euler equations directly yields the unsteady air forces instead of having to extract them by Fourier analysis from a full Euler solution.

3) Any fast and convenient explicit or implicit solution method for steady flows may be applied.

4) The unsteady air forces may be used directly within the standard modal flutter calculations if wanted.

5) The computation time is reduced by an order of magnitude (in our case by a factor of 10) saving costs and accelerating the analysis.

6) Comparison of results from full Euler equations and SDEu has proven to be excellent.

7) The method is applicable to subsonic, supersonic, and, in particular, transonic flow regimes.

References

[1]"Numerical Unsteady Aerodynamic and Aeroelastic Simulation," AGARD-R-822, 1997.

[2]Slooff, J. W., and Schmidt, W., ed., "Computational Aerodynamics Based on the Euler Equations," AGARD-AG-325, 1994.

[3]Knipfer, A., "Numerische Untersuchung der transsonischen Strömungen an schwingenden Triebwerksgondeln," Dissertation, Institut für Aeroelastik, DLR, Göttingen, Germany, Nov. 1995.

[4]Hall, K. C., "A Linearized Euler Analysis of Unsteady Flows in Turbomachinery," Ph.D. Dissertation, Massachusetts Inst. of Technology, Cambridge, MA, 1987.

[5]Hall, K. C., and Crawley, E. F., "Calculation of Unsteady Flows in Turbomachinery Using the Linearized Euler Equations," *AIAA Journal*, Vol. 27, No. 6, 1989, pp. 777–787.

[6]Hall, K. C., and Clark, W. S., "Calculation of Unsteady Linearized Euler Flows in Cascades Using Harmonically Deforming Grids," *Unsteady Aerodynamics, Aeroacoustics, and Aeroelasticity of Turbomachines and Propellers*, edited by H. M. Atassi, Springer-Verlag, New York, 1991, pp. 195–212.

[7]Hall, K. C., and Clark, W. S., "Linearized Euler Predictions of Unsteady Aerodynamic Loads in Cascades," *AIAA Journal*, Vol. 31, No. 3, 1992, pp. 540–550.

[8]Holmes, D. G., and Chuang, H. A., "2D Linearized Harmonic Euler Flow Analysis for Flutter and Forced Response," *Unsteady Aerodynamics, Aeroacoustics, and Aeroelasticity of Turbomachines and Propellers*, edited by H. M. Atassi, Springer-Verlag, New York, 1991, pp. 213–230.

[9]Zirkelbach, J., "Lösung der zeitlinearisierten Eulergleichungen für schwingende Schaufelgitter in Quasi-3D Strömung," Dipl.-Ing. Thesis, Lehrstuhl für Fluidmechanik, TUM-LSM 90/26, Technische Universität München, Garching, Germany, April 1990.

[10]Kahl, G., and Klose, A., "Time Linearized Euler Calculations for Unsteady Quasi-3D Cascade Flows," *Unsteady Aerodynamics, Aeroacoustics, and Aeroelasticity of Turbomachines and Propellers*, edited by H. M. Atassi, Springer-Verlag, New York, 1991, pp. 109–126.

[11]Hall, K. C., and Lorence, C. B., "Calculation of Three-Dimensional Unsteady Flows in Turbomachinery Using the Linearized Harmonic Euler Equations," *Journal of Turbomachinery*, Vol. 115, No. 4, 1993, pp. 800–809.

[12]Hall, K. C., Clark, W. S., and Lorence, C. B., "A Linearized Euler Analysis of Unsteady Transonic Flows in Turbomachinery," *Journal of Turbomachinery*, Vol. 116, No. 3, 1994, pp. 477–488.

[13]Lindquist, D. R., "Computation of Unsteady Transonic Flowfields Using Shock Capturing and Linear Perturbation Euler Equations," Ph.D. Dissertation, Massachusetts Inst. of Technology, Cambridge, MA, 1992.

[14]Lindquist, D. R., and Giles, M. B., "Validity of Linearized Unsteady Euler Equations with Shock Capturing," *AIAA Journal*, Vol. 32, No. 1, 1994, pp. 46–53.

[15]Roe, P. L., "Approximate Riemann Solvers, Parameter Vectors and Difference Schemes," *Journal of Computational Physics*, Vol. 43, No. 2, 1981, pp. 357–372.

[16]Kreiselmaier, E., "Berechnung instationärer Tragflügelumströmungen auf der Basis der zeitlinearisierten Eulergleichungen," Dissertation, Lehrstuhl für Fluidmechanik, Technische Universität München, Garching, Germany, July 1998.

[17]Huber, T., and Rochholz, H., "Instationäre Strömungen an Tragflächen und Körpern, Kompressible Strömungen," Lehrstuhl für Fluidmechanik, TUM-LSM 90/66, Technische Universität München, Garching, Germany, Nov. 1990.

[18]Haase, W., Chaput, E., Elsholz, E., Leschziner, M. A., Müller, U. R., (ed.), *ECARP—European Computational Aerodynamics Research Project: Validation of CFD Codes and Assessment of Turbulence Models*, Vieweg, Braunschweig, Germany, 1997, pp. 479–500.

[19]Whitfield, D., and Janus, J., "Three Dimensional Unsteady Euler Equations Solution Using Flux Vector Splitting," AIAA Paper 84-1552, 1984.

[20]Jameson, A., and Turkel, E., "Implicit Schemes and LU-Decompositions," *Mathematics of Computation*, Vol. 37, No. 156, 1981, pp. 385–397.

[21]Harten, A., "On a Class of High Resolution Total-Variation-Stable Finite Difference Schemes," *SIAM Journal on Numerical Analysis*, Vol. 21, No. 1, 1984, pp. 1–23.

[22]Yee, H. C., "A Class of High Resolution Explicit and Implicit Shock Capturing Methods," NASA TM 101088, NASA Ames Research Center, 1989.

[23]Davis, S. D., "NACA64A010 (NASA Ames Model) Oscillatory Pitching, Compendium of Unsteady Aerodynamic Measurements," AGARD-R-702, AGARD, 1982.

[24]King, L. S., and Johnson, D. A., "Calculations of Transonic Flow About an Airfoil in a Wind Tunnel," AIAA Paper 80-1366, 1980.